Design and Validation of a Torque-Controllable Series Elastic Actuator-Based Hip Exoskeleton for Dynamic Locomotion

Inseung Kang *
Department of Brain and Cognitive Sciences
Massachusetts Institute of Technology
Cambridge, MA 02139
Email: inseung@mit.edu

Reese R. Peterson
School of Mechanical Engineering
Georgia Institute of Technology
Atlanta, GA 30332
Email: rpeterson37@gatech.edu

Kinsey R. Herrin
School of Mechanical Engineering
Georgia Institute of Technology
Atlanta, GA 30332
Email: kinsey.herrin@me.gatech.edu

Anirban Mazumdar
School of Mechanical Engineering
Georgia Institute of Technology
Atlanta, GA 30332
Email: anirban.mazumdar@me.gatech.edu

Aaron J. Young
School of Mechanical Engineering
Georgia Institute of Technology
Atlanta, GA 30332
Email: aaron.young@me.gatech.edu

Series elastic actuators (SEAs) are increasingly popular in wearable robotics due to their high fidelity closed-loop torque control capability. Therefore, it has become increasingly important to characterize its performance when used in dynamic environments. However, the conventional design approach does not fully capture the complexity of the entire exoskeleton system. These limitations stem from identifying design criteria with inadequate biomechanics data, utilizing an off-the-shelf user interface, and applying a benchtop-based PID control for actual low-level torque tracking. While this approach shows decent actuator performance, it does not consider human factors such as the dynamic back-driving nature of human-exoskeleton systems as well as soft human tissue dampening during the load transfer. Using holistic design guidelines to improve the SEA-based exoskeleton performance during dynamic locomotion, our final system has an overall mass of 4.8 kg (SEA mass of 1.1 kg) and can provide a peak joint torque of 108 Nm with a maximum velocity of 5.2 rad/s. Additionally, we present a user state-based feedforward controller to further improve the low-level torque tracking for diverse walking conditions. Our study results provide future exoskeleton designers with a foundation to further improve SEA-based exoskeleton's torque tracking response for maximizing human-exoskeleton performance during dynamic locomotion.

Keywords: Exoskeleton, Series Elastic Actuator, Torque Control, Dynamic Locomotion

1 Introduction

Exoskeleton technology has recently shown promising results for augmenting humans for enhanced mobility during locomotion [1, 2]. Both able-bodied and clinical populations can potentially benefit from this technology due to its wide range of applications, such as augmenting human physical capabilities [3, 4, 5, 6], partially assisting during community ambulation [7, 8, 9], and restoring physical attributes through rehabilitation [10, 11, 12]. Most of these robotic exoskeletons utilize actuators to provide assistance during locomotion that is co-axially aligned with the user's biological joint. While several types of actuators can be implemented for exoskeleton applications (e.g., pneumatic [13] and hydraulic actuators [14]), electromechanical actuators are the most common type. This is largely due to having a high power-to-weight ratio and an energy source that is comparatively lightweight and safe. Additionally, literature has indicated that minimizing mass added to the user's body plays a critical role in the overall human exoskeleton performance (e.g., reducing the energetic cost of walking) [15].

A commonly used actuator type to achieve closed-loop

*Address all correspondence for other issues to this author.

torque control is a series elastic actuator (SEA), where an elastic element is located in series between the actuator's output and the payload. By measuring the deflection of the elastic element, the torque applied at the actuator can be accurately measured [16, 17]. Several research studies have utilized SEAs for robotic exoskeleton applications [18, 19, 20, 21, 22, 23]. Conventionally, these exoskeletons integrate a rotary SEA around the targeted joint and provide joint torque in the sagittal plane. However, the majority of these studies were often limited as the torque tracking performance was only validated at low assistance magnitude and walking speed conditions, which does not resemble what humans experience during regular locomotion. The conventional method to optimize the SEA torque response in closed-loop feedback control is proportional-integral-derivative (PID) control. Most of these PID controllers for an SEA are empirically tuned in a benchtop setting to evaluate the actuator's torque bandwidth. While these 'tuned' controllers may perform well in a static setting, these controllers often exhibit poor torque tracking performance when used on humans during locomotion. This is mainly due to the benchtop-based actuator optimization procedure not sufficiently capturing the physical interaction realized during dynamic tasks performed by a human. Several factors can affect torque tracking results such as the actuator output being constantly back-driven during dynamic locomotion (whereas benchtop is done on a locked rotor) and the user's interface limiting load transfers from the actuator to the human's musculoskeletal structure [24, 25, 26]. Literature has investigated the optimization of low-level control approaches in exoskeletons to yield high fidelity closed-loop feedback control [27]. Although the conventional approach of pure feedback control is convenient, large PID gains can cause instability in the system during operation. Fortunately, the addition of a feedforward control strategy based on user state information can reduce the controller effort within the feedback loop. Zhang *et al*. investigated the addition of a feedforward gain for level-ground walking to improve the performance of a cable-driven exoskeleton actuator [28]. While low-level controller optimization is a promising direction for improving actuator performance, this approach has not been explored for other locomotion modes (e.g., ramps and stairs) as well as the intensity of such modes (e.g, walking speed and assistance level). A more in-depth analysis of the control strategies and their generalizability to these modes need to be explored to further understand their efficacy.

In this study, we have improved the torque tracking performance of an SEA-driven robotic hip exoskeleton, shown in Fig. 1, by optimizing both the mechanical design and the low-level control architecture. To meet the mechanical design criteria, we developed a robust harmonic drive-based SEA using a titanium torsion spring to maximize the power-to-weight ratio. Additionally, we customized the user interface to improve power transfer from the SEA to the user's limbs and torso. For the control architecture, we incorporated an additional user state-based feedforward controller to the baseline PID controller. This further improved the overall torque tracking performance during dynamic locomotion under three conditions: 1) varying walking speed, 2) varying assistance magnitude, and 3) different locomotion modes. The key contributions of this study are 1) the development of a lightweight SEA-based robotic hip exoskeleton with high torque bandwidth capabilities for dynamic locomotion and 2) the improvement of torque tracking performance on the SEA-driven human-exoskeleton robotic platform across distinct terrains with varied assistance conditions. These study findings can be a foundational guideline for future exoskeleton designers to design a more robust SEA-based exoskeleton that can maximize torque tracking performance in various locomotion conditions. This will push the field forward to develop exoskeletons that can translate from a laboratory environment to real-world scenarios.

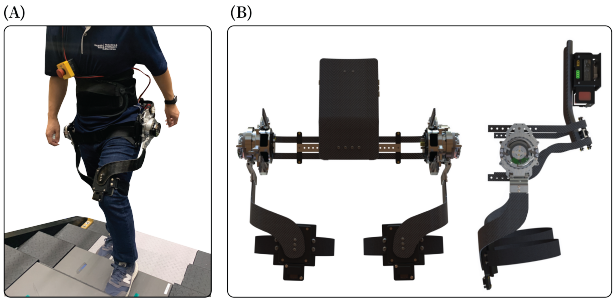

Fig. 1. Series elastic actuator-driven robotic hip exoskeleton. (A) The exoskeleton provides flexion and extension assistance at the hip joint bilaterally in the sagittal plane for multimodal locomotion. (B) The exoskeleton houses different on-board mechanical sensors to measure the user's limb kinematics during locomotion.

2 Robotic Hip Exoskeleton Design

2.1 Series Elastic Actuator

2.1.1 Actuator Design Specification

The main objective of our design was to develop an exoskeleton system capable of providing a peak torque of 120 Nm, maximum continuous torque of 55 Nm, and peak angular velocity of 4.5 rad/s to accommodate dynamic human locomotion (equivalent to 100% of the biological torque for an average user) for wide ranges of body sizes. A detailed illustration of the proposed actuator design is shown in Fig. 2. These target requirements for our SEA were based on human gait biomechanics data [29, 30, 31], where we analyzed the hip joint biomechanics of an average male in the United States [32] across 5 locomotion modes: level ground (LG), ramp ascent (RA), ramp descent (RD), stair ascent (SA), and stair descent (SD) at a wide range of walking speeds. To that end, we analyzed the fastest walking speed (up to 1.6 m/s) at each given mode to examine the required hip joint torque and speed. During extreme scenarios (e.g., fast LG and steep RA), humans exhibit a peak hip joint moment of 1.3 Nm/kg, nominal joint torque of 0.6 Nm/kg (relating to the maximum continuous torque), and peak joint angular velocity of 4.4 rad/s.

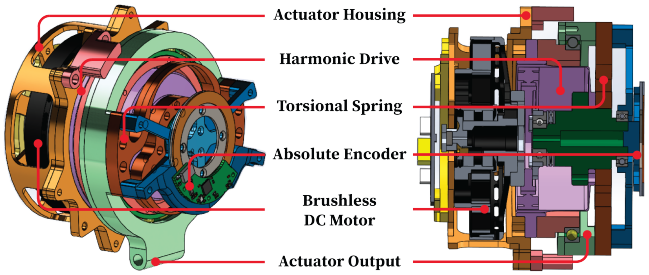

Fig. 2. Harmonic drive-based series elastic actuator. The brushless DC motor is coupled with the 50:1 Harmonic Drive gear transmission. The output torque is calculated via titanium torsional spring deflection measured with the absolute encoder.

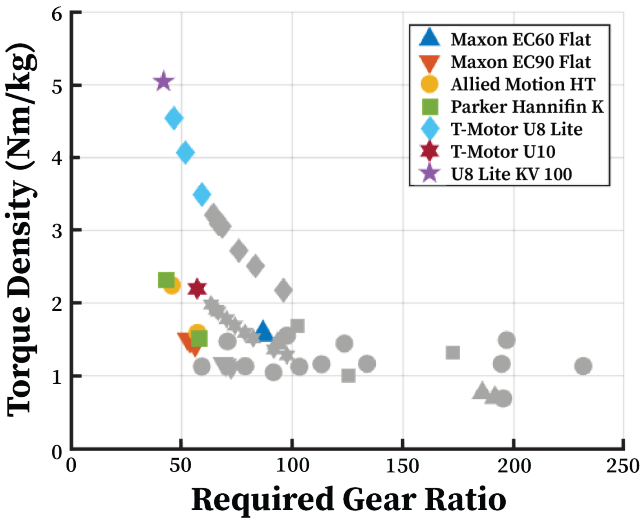

Fig. 3. Motor comparison of torque density relative to the required gear ratio. Torque density is defined as max continuous torque divided by motor mass, and the required gear ratio is determined from desired max continuous torque. Colored data points represent the optimal motor from specific motor manufacturers per series. The selected motor (T-Motor's U8 Lite KV100) has the highest torque density at the lowest required gear ratio.

2.1.2 Motor and Gear Component Optimization

Historically, the field has not systematically analyzed different motor specifications when designing an SEA-based exoskeleton, but selected a commonly used motor in previous actuator designs. For example, SEAs have utilized a brushless DC (BLDC) motor with a high gear reduction to minimize overall mass. However, this approach is suboptimal as a high ratio gear transmission can amplify nonlinearities such as backlash and friction. Moreover, reflected inertia from the output shaft to the motor can overburden the motor driver (due to the generation of back electromotive force). Recently, advancements in the drone industry led to the development of high torque density motors (large motor constant with high pole pairs), allowing a reduced gear ratio.

We analyzed motors from various manufacturers (design review in July 2020) commonly used in SEA designs to choose the motor that best met our design specification of high torque density (2 Nm/kg or greater) and low gear ratio transmission (less than 75:1) while having low mass. We excluded motors with mass greater than 650 g and the required gear ratio (calculated from desired nominal torque) of greater than 250:1 as they deviated too much from our design specification. From our analysis, the optimal BLDC motor for our application was T-Motor's U8 Lite KV100 (T-Motor, China) as shown in Fig. 3. Of the motors in our analysis, our chosen motor had the highest torque density at the lowest required gear ratio. Our selected motor had a torque constant of 0.09 Nm/A, maximum continuous torque of 1.08 Nm, peak torque of 2.61 Nm, and peak angular velocity of 251.3 rad/s with an overall mass of 238 g. While peak angular velocity and peak torque were common specifications in motor data sheets, they can be deceiving as a high peak angular velocity implies a low peak torque due to the inverse relationship between motor speed and torque. Therefore, we did not use peak values in our motor analysis and evaluated the motors using nominal parameters only.

An SEA can have several types of mechanisms for the gear transmission such as planetary gear, worm gear, and ball screw drive train. However, these gear systems have limitations such as gear backlash, friction within the transmission, and large mass. The harmonic drive is a state-of-the-art gear transmission mechanism that has a high torque output with zero backlash. Based on the results from the motor comparison, we chose a harmonic drive with a 50:1 gear ratio (CSF-25-50-2A-GR-LW, Harmonic Drive Systems, Japan) to be coupled with the selected motor.

An important feature to consider in SEA design optimization is the joint angular velocity response of the actuator during torque assistance. This is mainly due to the angular velocity being related to the required battery voltage during operation. As the SEA torque control is achieved using current control through a servo driver, the angular velocity (relating to the operating motor voltage) is dependent on the amount of current being commanded since the user's joint is non-static during the gait cycle. To fully validate that the specified motor and gear system achieves the desired torque and speed requirements, we utilized the following equation to model the SEA voltage response.

$$V_m = \frac{\tau_m}{k_t} R_m + k_e \omega_m \tag{1}$$

where V_m is the motor voltage, τ_m is the motor torque, k_t is the motor torque constant, R_m is the motor winding resistance, k_e is the motor voltage constant, and ω_m is the joint angular velocity. Using Eq. 1, we simulated the SEA's voltage response when providing maximum assistance level across 5 locomotion modes at 1.2 m/s (using the gait biomechanics data). The simulation results indicated that the SEA is well below the operating voltage requirement of the motor (24 V) across all locomotion modes (Supplemental Document).

2.1.3 Spring Stiffness Evaluation

A key factor for improving the SEA torque tracking performance is to increase the resolution of the spring deflection. This can be achieved by increasing the encoder reading resolution and reducing the spring stiffness such that the spring deflects more with a given torque input. However, increasing the elasticity decreases the end effector's torque tracking bandwidth. Hence, an optimal elasticity with a high encoder reading resolution is needed to maintain the desired torque bandwidth. To maximize the spring deflection resolution, we utilized a 19-bit absolute magnetic encoder at the actuator output (AksIM, RLS, Slovenia).

Several types of elastic elements have been investigated in previous SEA studies [33]. Oftentimes, metal-based springs (steel or aluminum) are used for their reliable spring stiffness linearity which is a critical aspect in the SEA low-level control. To further reduce the form factor while maintaining high torque output capabilities, we utilized a custom titanium-based torsional spring based on the original design from [34]. We experimentally validated that the spring exhibited a linear response within the operating range of $\pm$ 20 Nm. A benchtop setup and testing results for spring stiffness validation is shown in Fig. 4. The spring stiffness of our SEA was determined to be 593 Nm/rad with a torque reading resolution of 0.007 Nm.

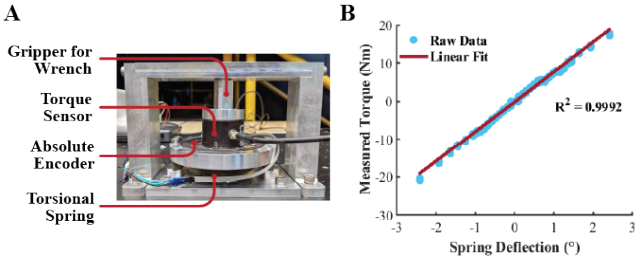

Fig. 4. Spring stiffness validation results. (A) Benchtop setup is utilized to obtain (B) experimental data. Different magnitudes of torque are applied to the test rig bidirectionally while a torque sensor and an absolute encoder measured the spring deflection. Experimental spring stiffness was measured to be 593 Nm/rad.

2.1.4 Final Series Elastic Actuator Specification

After these design optimization processes, we finalized the SEA design as shown in Fig. 5A. When fully assembled, each SEA is capable of reaching 108 Nm of peak torque, 60 Nm of continuous torque, and 5 rad/s peak velocity while weighing 1112 g. While the actuator can theoretically operate up to a peak torque of 130.5 Nm, the motor driver's peak current limitation was set to 24A, reducing the output peak torque capability to 108 Nm as shown in Table. 1. The actuator has 130° range of motion (100°/30° hip flexion/extension) in the sagittal plane and 30° range of motion (15°/15° hip abduction/adduction) in the frontal plane.

2.2 Electronic Components

The exoskeleton is comprised of different mechanical sensors which control the overall system as depicted in Fig. 5B. All control loops are operated on an onboard microcontroller equipped with an FPGA layer (myRIO, National Instruments, USA). A 19-bit absolute magnetic rotary encoder is located at the actuator output, with the magnetic ring connected before the spring and the read head connected after to read the relevant spring deflection. 6-axis inertial measurement units (MPU-9250, InvenSense, USA) are placed on the trunk and each thigh cuff to measure the user's limb acceleration and gyroscope data. All mechanical sensors communicate with the microcontroller via SPI communication. An STM32 microcontroller-based motor driver (T-motor, China) servos the motor using a 12-bit encoder for commutation while communicating with the microcontroller via CAN bus using an MCP2515 CAN-SPI conversion chip. All sensors and motors are powered by a 22.2 V 3600 mAh LiPo battery (Venom Fly, Venom Power, USA) which allows the exoskeleton to have an approximate run-time of 2 hours (continuous operation of 15 Nm assistance level). All sensor reading and low-level control are handled at the FPGA level running at 1 kHz while the high-level controller is implemented using the real-time target layer running at 500 Hz.

2.3 Custom User Interface

To make the exoskeleton portable and comfortable, a dedicated human orthosis was manufactured. The design consists of a carbon fiber backplate with an integrated lumbar curve attached to a circumferentially adjustable lumbosacral orthosis (LSO) in addition to customized tapered elastic straps, both of which secure to the user's body to optimally transfer the weight of the exoskeleton directly to the user's hip and waist area. During development, anthropometric factors were considered to ensure a close and comfortable fit for users with various stature and body sizes. We mainly focused on the 99th percentile male hip width of 393 mm and 50th percentile female hip width of 341 mm. In our previous designs [37, 36], the maximum mediolateral dimension was capped at 410 mm which led to challenges in fitting a more diverse subject pool. Therefore, for our current design, we increased the mediolateral dimension capability by over 100 mm while still allowing the capture of a smaller human subject, resulting in mediolateral adjustability of 173 mm (345 $\sim$ 518 mm) and anteroposterior adjustability of 100 mm (90 $\sim$ 190 mm).

2.3.1 Sliding Thigh Cuff

In order to interact smoothly with the user, exoskeletons must allow a full range of motion during movement. However, it is nearly impossible to perfectly align and maintain the rotational axis of the exoskeleton in line with the user's hip joint throughout the gait cycle due to the wide range of motion during locomotion. To mitigate this, we designed a thigh cuff to automatically compensate for the kinematic mismatch between the user's thighs and exoskeleton, elim-

Table 1. Series Elastic Actuator Design Metric

Design Criteria	Target Value	Giovacchini *et al.*	Zhang *et al.*	Kang *et al.*	Final Design
Peak Joint Torque	120 Nm	35 Nm	80 Nm	30 Nm	108 Nm
Max Continuous Torque	55 Nm	N/A	40 Nm	15 Nm	60 Nm
Peak Angular Velocity	4.5 rad/s	6.98 rad/s	2.62 rad/s	5.2 rad/s	5 rad/s
Range of Motion (Sagittal/Frontal)	130°/30°	140°/40°	128°/41°	130°/30°	130°/30°
Gear Ratio	75:1	80:1	100:1	100:1	50:1
Actuator Mass	1.5 kg	1.2 kg	1.5 kg	0.9 kg	1.1 kg

To compare our final design to relevant SEA-based exoskeletons, we have included comparable exoskeleton designs from the literature [20, 35, 36]. Note that only the SEA-based hip exoskeleton designs were included as the benchmark.

inating user discomfort caused by shear forces against the skin during locomotion. The thigh cuff unit incorporates an aluminum slider that is captured by inner and outer covers made out of carbon fiber-filled nylon as shown in Fig. 5C. Two elastic bands connect this aluminum slider to four dowel pins extruded from the cover. This integrated slider allows the thigh cuff to move 25 mm and 10 mm in the proximodistal and mediolateral direction, respectively. The fully assembled thigh cuff is coupled with a carbon fiber-based upright contoured to the user's thigh. The thigh upright was fabricated from the epoxy acrylic resin using standard composite wet lamination techniques under vacuum. The upright was fabricated with a bidirectionally woven carbon and a unidirectional carbon tape layered at 90° and 0° orientations. Additional carbon fiber was placed into the layup at the junction between the SEA and the upright to prevent mechanical failure during load transfer.

2.3.2 C-Channel Frame

The C-Channel is the human interface that connects the SEA to the LSO which conforms to the user's body shape as illustrated in Fig. 5D. The C-Channel consists of four custom manufactured carbon fiber pelvic struts and a size adjustable aluminum plate. The carbon fiber pelvic struts are connected with the aluminum plate posteriorly via aluminum-based couplers. All four pelvic struts were fabricated similarly to thigh cuffs.

2.3.3 Flexible Pelvic Orthosis

The pelvic orthosis incorporated in the exoskeleton design utilized an enhanced profile LSO (SLEEQ AP+, Thuasne, USA). This LSO was chosen for its comfort and improved user compliance and outcomes while accommodating a wide range of body sizes. It provides appropriate compression and support for the lower back, helping the exoskeleton to conform better to the user's body and preventing the exoskeleton from moving relative to the user as shown in Fig. 5E. This LSO was integrated into a custom-designed carbon fiber backplate (Fillauer, USA) based on our previous study on the user interface's impact on the overall exoskeleton performance [26]. When fully assembled, the exoskeleton system has a total mass of 4.78 kg as shown in Table. 2.

Table 2. Overall Exoskeleton Mass Distribution

Component	Mass (g)
Series Elastic Actuator (×2)	2224
Electronics Backback	471
Li-Po Battery	392
C-channel Frame	335
Flexible Pelvic Orthosis	713
Thigh Interface (×2)	642
Total Mass	**4777**

3 Exoskeleton Control Strategy

3.1 Biological Torque Controller

The exoskeleton incorporated a three-tier control approach presented in our previous work where the high-level estimated the user's state, the mid-level generated relevant torque profile, and the low-level ensured a reliable torque tracking [37]. The exoskeleton incorporated a biological torque controller in which the commanded assistance profile was based on the human biological hip joint moment during locomotion [38]. The overall control approach ensures to generate a joint torque profile that is in line with the user's biological joint demand (e.g., flexion torque when the user exerts flexion joint moment) during the gait cycle. This controller was used since it is an effective assistance strategy for augmenting human walking [37, 39, 40]. To ensure continuous assistance, each profile was fit to the corresponding joint torque profile using a sum of univariate Gaussians. Given the current gait phase x, the desired assistance torque τ was com-

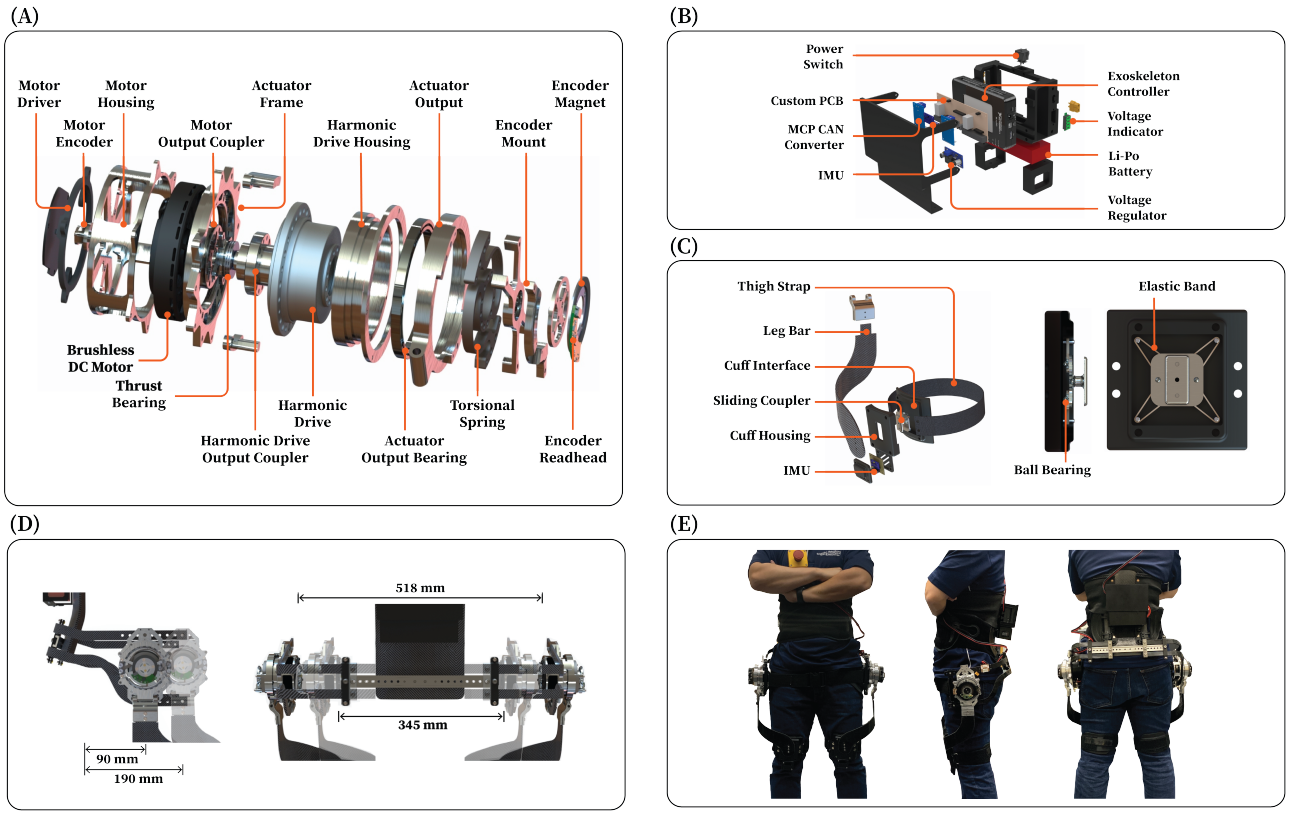

Fig. 5. Robotic hip exoskeleton design. (A) Exploded view of the harmonic drive-based series elastic actuator design. The brushless DC motor is coupled with the 50:1 harmonic drive gear transmission. Titanium-based torsional spring deflection at the output shaft is measured via an absolute encoder for closed-loop torque control. (B) Exploded view of the electronics backpack unit. The backpack houses a microcontroller, a custom printed circuit board for signal routing, and a Li-Po battery to power the exoskeleton. (C) Close-up view of the sliding thigh interface unit. The aluminum-based slider uses ball bearings to minimize friction between the cover surfaces. The elastic bands allow the slider to passively return to the original location when not engaged. (D) Carbon fiber-based C-channel frame design. The C-channel has adjustability in both anteroposterior and mediolateral direction to accommodate different body sizes. (E) Final assembly of the series elastic actuator-based robotic hip exoskeleton design. All components are integrated for autonomous control.

puted using the locomotion mode-specific coefficients (a, μ, and σ) using Eq. 2,

$$\tau = \sum_{i=1}^{n} a_i \mathcal{N}(x, \mu_i, \sigma_i) \tag{2}$$

where the Gaussian distribution $\mathcal{N}$ was defined as

$$\mathcal{N}(x, \mu, \sigma) = e^{-\frac{1}{2}(\frac{x-\mu}{\sigma})^2} \tag{3}$$

Using the magnitude shaping coefficient a (which proportionally scales the overall profile), we tuned the flexion and extension peak torque to match the peak human biological joint moment. Additionally, we tuned timing coefficients such as peak timing, μ, and assistance duration, σ, to align the assistance profile to human biomechanics. Illustration of desired exoskeleton assistance profiles for different locomotion modes is shown in Fig. 6. The gait phase was estimated using a time-based estimation method which is an analytical approach using a force sensitive resistor placed on the user's heel [37]. We linearly interpolated the user's gait phase by dividing the time since the most recent heel contact by the user's average stride duration from the previous two gait cycles.

3.2 Low-Level Control

For the exoskeleton, the torque tracking performance of two low-level controllers was evaluated. (1) a PID controller which serves as the baseline and (2) the same PID controller from (1) with an additional user state-based feedforward controller. Controller gains for the PID approaches were tuned and the tracking performance was evaluated on a benchtop setting before human subject testing. Benchtop evaluation consisted of a standard sinusoidal chirp signal sweep test ($\pm$ 30 Nm, 0.1 $\sim$ 100 Hz for 10 seconds) to determine the actuator's torque bandwidth. A benchtop setting for the SEA torque bandwidth validation is shown in Fig. 7.

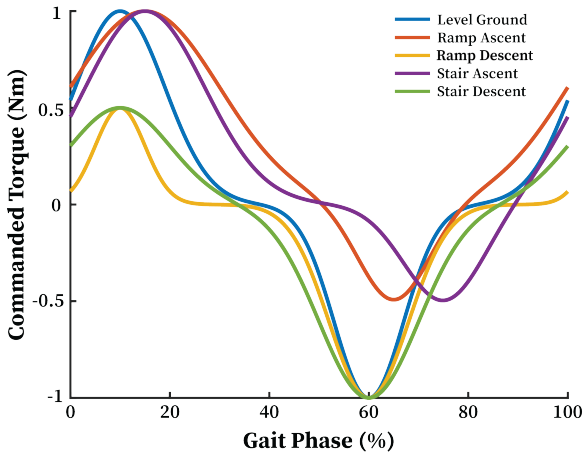

Fig. 6. Biological torque controller using a sum of univariate Gaussians. Reference hip assistance profile can be shaped using different tuning parameters to match the human biological hip joint moment. Five colored lines represent assistance profiles for different locomotion modes.

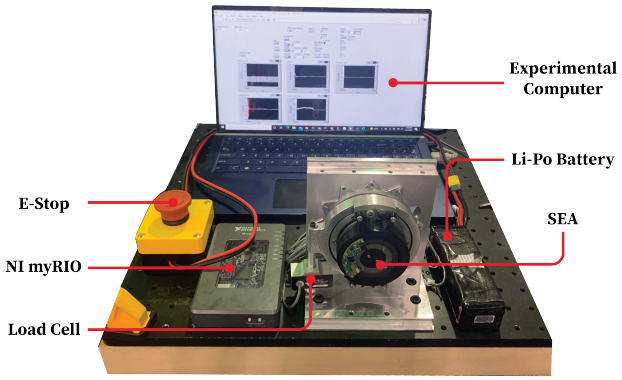

Fig. 7. Benchtop setting for series elastic actuator torque bandwidth validation. The actuator is mounted on a test stand with its output fixed. The microcontroller servos the motor where a load cell connected in series to recorded the output torque.

3.2.1 PID Control

The conventional approach for low-level torque control in powered exoskeletons has been model-free control due to its simplicity in tuning for control gains in a benchtop setting [20, 23]. More specifically, model-free PD control has shown decent tracking performance. However, due to static friction in the system, steady-state errors can arise during dynamic movement. To mitigate this, an integral term can be incorporated to eliminate residual errors. The PID control approach in this study uses a derived plant model to simulate the system and optimizes the controller gains based on the system response using Simulink (MATLAB, MathWorks, USA). An example of the SEA dynamic model is illustrated in Fig. 8.

From the SEA dynamic model, the general dynamics of the motor and load were derived to be Eq. 4 and Eq. 5,

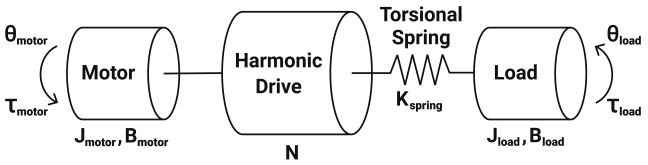

Fig. 8. Series elastic actuator dynamic model. The model consists of a motor that provides an input torque, a harmonic drive to amplify the input torque, a torsional spring to measure the output torque for closed-loop feedback, and a load that represents a human hip joint.

respectively.

$$J_{motor}\ddot{\theta}_{motor} = \tau_{motor} - \frac{1}{N}\tau_{spring} - B_{motor}\dot{\theta}_{motor} \tag{4}$$

$$J_{load}\ddot{\theta}_{load} = \tau_{spring} + \tau_{load} - B_{load}\dot{\theta}_{load} \tag{5}$$

Additionally, Eq. 6 and Eq. 7 can be used to describe the spring behavior,

$$\tau_{spring} = K_{spring}\theta_{spring} \tag{6}$$

$$\theta_{spring} = \frac{1}{N}\theta_{motor} - \theta_{load} \tag{7}$$

where J_{motor} and J_{load} are the moments of inertia of the motor and load, B_{motor} and B_{load} are the damping coefficients of the motor and load, and θ_{motor} and θ_{load} are the angular positions of the motor and load. N is the gear ratio of the harmonic drive, K_{spring} is the torsional spring constant, and θ_{spring} is the spring deflection. τ_{motor} is the input torque from the motor, τ_{spring} is the output torque transmitted through the spring, and τ_{load} is the external disturbance torque from the interaction between the human leg and exoskeleton. Utilizing these equations, the plant model $G(s)$ is represented by the transfer function between the input motor torque $\tau_{motor}(s)$ and output spring torque $\tau_{spring}(s)$. After understanding the entire system model, we initially evaluated the plant model $G(s)$. Through a standard simulation, we identified the final transfer function's number of poles and zeros to be 3 and 1, respectively. Using the experimental data from an open-loop sine sweep on the benchtop setting, we estimated the transfer function of the SEA dynamic model based on $G(s)$. With the identified $G(s)$, the system was simulated and tuned within Simulink to obtain optimized PID control gains. The control gains were then tested on the physical system and further refined. From the benchtop testing, the SEA's torque bandwidth of the fitted plant model and the tuned PID transfer functions were determined to be 6 Hz and 12 Hz, respectively. A bode plot of the SEA torque bandwidth testing is shown in Fig. 9.

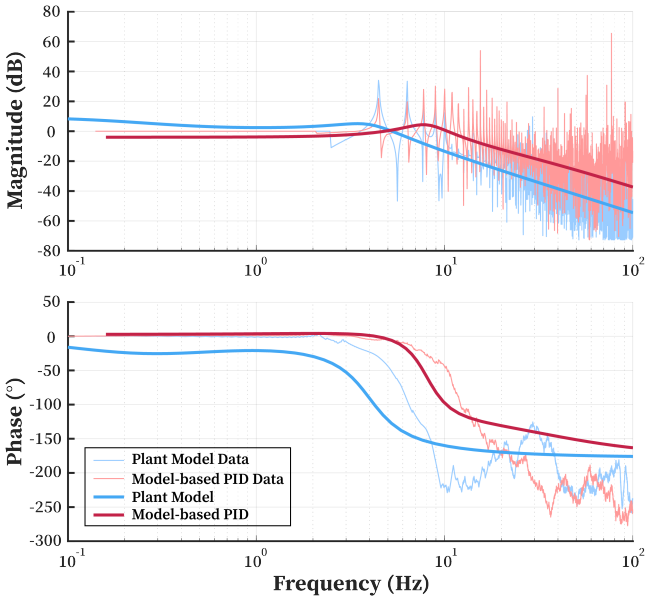

Fig. 9. Series elastic actuator torque bandwidth result. A sine chirp ranging from 0.1 $\sim$ 100 Hz was commanded with 30 Nm peak torque to characterize the actuator system. The PID controller's transfer function showed a 12 Hz cut-off frequency (plant model 6 Hz).

4 Exoskeleton Performance Validation

4.1 Experimental Protocol

We recruited three able-bodied subjects with an average age of 24.7 $\pm$ 5.7 years, height of 1.81 $\pm$ 0.08 m, and body mass of 97.8 $\pm$ 32.5 kg to experimentally validate the torque tracking response of our robotic hip exoskeleton. The study was approved by the Georgia Institute of Technology Institutional Review Board and informed written consent was obtained for all subjects. Three conditions were used to evaluate the assistance torque tracking while the subject walked with the hip exoskeleton, as illustrated in Fig. 10.

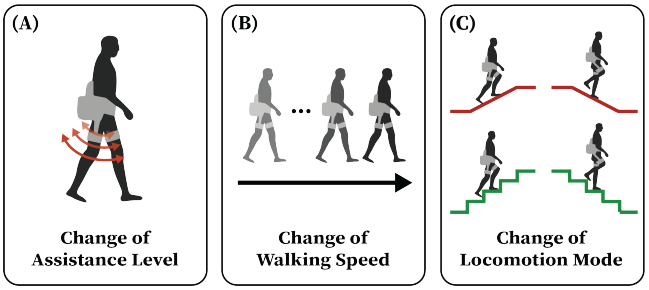

Fig. 10. Human subject testing conditions for validating the exoskeleton torque tracking performance. (A) varying assistance magnitude at an average walking speed on a treadmill. (B) providing nominal assistance while varying walking speeds. (C) nominal assistance while navigating in different locomotion modes.

Condition 1 (C1) was level-ground walking on a treadmill (TuffTread, USA) at 1.2 m/s at assistance magnitudes ranging from 0 Nm to 20 Nm with a 5 Nm increment every 30 seconds using the biological torque controller for a total of 5 trials. Condition 2 (C2) was level-ground walking on a treadmill at walking speeds ranging from 0.8 m/s to 1.6 m/s with a 0.2 m/s increment every 30 seconds with 10 Nm assistance magnitude for a total of 5 trials. Condition 3 (C3) varied locomotion modes where the subject navigated a simulated terrain park that included 5 locomotion modes (LG, RA, RD, SA, and SD) while walking at a preferred walking speed. The terrain park was set to a nominal height conventionally used in an industry setting (ramp at 11° slope and stair at 15.24 cm height). Each subject navigated the terrain park and walked at all five modes 3 times each, for a total of 15 trials. During locomotion, the assistance level was set to 10 Nm for all modes. For all three conditions, we evaluated the SEA torque tracking performance using two control methodologies: the PID control with and without the user state-based feedforward control.

4.2 User State-Based Feedforward Control

The addition of a user state-based feedforward controller can reduce the overall tracking error during dynamic setpoint changes, alleviating control effort from the feedback loop. A user state-based feedforward controller is developed utilizing 3 different user's state information: assistance magnitude, walking speed, and locomotion mode. This feedforward function was computed from the exoskeleton torque tracking performance using the baseline PID controller. Initially, a 2nd order polynomial function was fitted to C1 and C2 results to understand the overall torque tracking trend across conditions. For two different conditions, the exoskeleton torque tracking error exhibited a quadratic growth (R^2 = 0.99) with an increase of assistance magnitude while a quadratic plateau (R^2 = 0.89) was shown with an increase of walking speed. Using this baseline function, a feedforward function was computed as a function of assistance magnitude, walking speed, and locomotion mode. Since 10 Nm at 1.2 m/s was the nominal assistance condition that was applicable to all three walking conditions, we expanded this feedforward function to C3 to compute a relevant feedforward gain for other locomotion modes (no clear trend was shown across different ambulation modes). We utilized the following equation along with the baseline PID controller to apply additional torque to the SEA,

$$\tau_{command} = \tau_{PID} + sgn(\tau_{PID}) \times k_{ff}(l_m)\tau_{ff} \tag{8}$$

where $\tau_{command}$ is the commanded torque, τ_{PID} is the torque output from the PID, k_{ff} is the mode-dependent gain, l_m is the locomotion mode, and τ_{ff} is the feedforward torque. τ_{ff} can be further expanded using Eq. 9,

$$\tau_{ff} = w(\tau_a + \tau_s) \tag{9}$$

where w is the weighting factor (equal weight between magnitude and speed) while τ_a and τ_s are the quadratic trend

as a function of assistance magnitude and walking speed based on the measured root mean square error (RMSE) from C1 and C2, respectively.

5 Human Subject Testing Results

Across all subjects, the SEA using the PID controller had 2.05 ± 1.37 Nm, 1.35 ± 0.19 Nm, and 1.07 ± 0.24 Nm RMSE for C1, C2, and C3, respectively. The torque tracking responses of the SEA for three walking conditions are shown Fig. 11. Using the feedforward gain, the SEA on average improved the torque tracking RMSE by 25.23 ± 8.66%, 18.45 ± 7.07%, and 16.43 ± 3.52% for C1, C2, and C3 across all subjects, respectively. The effect of feedforward gain on the SEA's torque tracking performance is shown in Fig. 11 and 12.

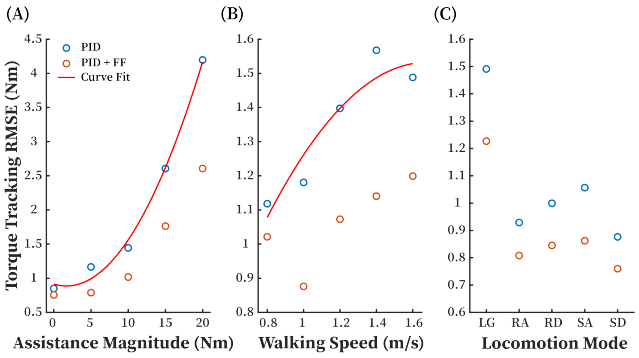

Fig. 11. Series elastic actuator torque tracking performance for (A) varying assistance magnitude, (B) varying walking speeds, and (C) different locomotion modes using the PID controller with (orange) and without (blue) the user state-based feedforward gain. After evaluating the PID controller's performance, a 2nd order polynomial function was fitted to the baseline torque tracking errors to generate a feedforward function.

6 Discussion

In this study, we introduced and validated a torque controllable SEA-based robotic hip exoskeleton design for dynamic locomotion. We optimized the design from multi-perspective analysis such as the actuator specification, spring design, user interface, and low-level control. The exoskeleton can provide a peak joint torque of 108 Nm in a wide walking speed range while only weighing 4.8 kg. While there are lighter hip exoskeletons available in the field (e.g., Samsung GEMS device with 2.1 kg), these devices are limited as they can only provide a small amount of torque and does not have torque tracking capability [41, 42]. Additionally, the integration of a streamlined custom user interface with minimal form factor enabled an efficient human-exoskeleton performance. Overall, the SEA-based hip exoskeleton was able to generate reliable joint torque assistance to the user across different locomotion modes and conditions.

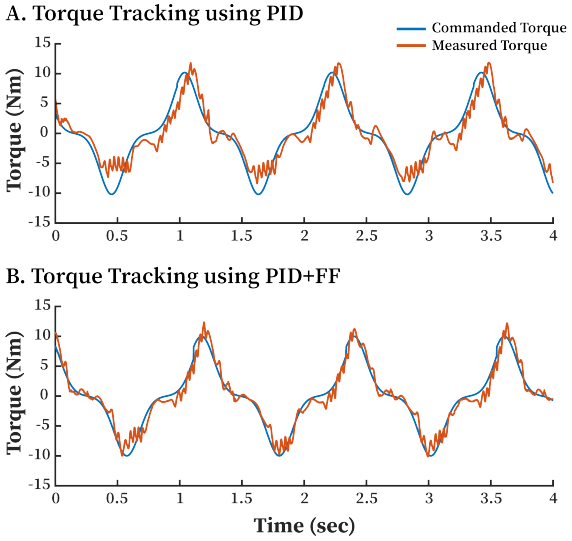

Fig. 12. Representative time series plot of the actuator torque tracking performance during level-ground walking at 1.2 m/s with 10 Nm assistance using the PID controller with and without the user state-based feedforward gain. Positive torque refers to a hip extension movement.

Indeed, integration of the user state-based feedforward gain was able to further improve the overall torque tracking performance of the SEA by 20% compared to the baseline. This result validated that the user state information is an important variable to consider even for low-level control.

A notable SEA-based hip exoskeleton design that has a similar design concept was done by Giovacchini *et al.* [20]. While this design also utilized a Harmonic Drive, the overall form factor was suboptimal as the SEA had an additional four-bar linkage transmission within the system. Additionally, the system did not utilize a high torque density motor resulting in a low peak torque capability (30% of our SEA). Another comparable exoskeleton design is done by Zhang *et al.* [35]. This 2-DOF hip exoskeleton design (frontal plane assistance) has the SEA with minimal form factor by tightly integrating a custom torsional spring. However, the design was still limited as it integrated an off-the-shelf interface and did not optimize auxiliary components (e.g., electronics backpack) which resulted in an overall mass of 10 kg. Considering these literature standards, our design achieved the state-of-the-art SEA-based hip exoskeleton as it optimized design criteria from several key factors that contribute to the overall human-exoskeleton performance.

For human applications, it was critical to accurately understand the relationship between the SEA torque RMSE and the user's state information (e.g., walking speed) to apply a relevant feedforward gain to the exoskeleton control. As illustrated in Fig. 11, the torque tracking RMSE increased with both the magnitude and speed, thus indicating a need for higher feedforward gains for higher magnitudes and speeds. One key feature that was noticed was that the overall trends of the torque tracking error for the magnitude and speed con-

ditions were different. While the increase in the subject's walking speed should have induced a greater load to the SEA performance due to the increase in the angular velocity demand, the resulting trend was different. Instead, the tracking error converged after a certain walking speed (approximately 1.4 m/s and higher). Since walking speed can be determined based on the subject's stride length and frequency, this result indicated that the subject may have converged to a certain stride frequency at a faster walking speed.

For different walking conditions, the applied gains were based on the feedforward function generated from the baseline PID performance. While it was possible to apply higher gains for all conditions, this approach did not exhibit a satisfactory performance as certain scenarios caused discomfort to the subject. This is because high feedforward gains can potentially induce instability (e.g., high gains on low assistance magnitude condition) as the overall system started to become a bang-bang control (small error in PID control being amplified). For the feedforward controller, we have applied a static gain for each state condition. While the proposed gain improved the baseline torque tracking as shown in Fig. 12B, residual torque tracking errors indicate that a more advanced feedforward controller is needed. For example, the controller can incorporate the user's gait phase information to scale the added feedforward term to correctly comprehend the high tracking error region.

One of the key limitations in the current field is the lack of holistic guidelines in designing an exoskeleton system. Typically, an exoskeleton design study focuses on the mechanical design of an actuator and neglects other important factors (e.g., user interface), which greatly limits the ability to design a system that can effectively provide assistance across a wide range of locomotor tasks. On the other hand, this study optimized the exoskeleton design from a multi-perspective design analysis, providing a foundational guideline for future developers. The extension of this study should focus on evaluating the exoskeleton performance on human outcome measures (with a higher subject number) such as metabolic cost and joint biomechanics.

7 Conclusion

In this work, we have designed and validated an autonomous SEA-based robotic hip exoskeleton for dynamic locomotion. Our proposed SEA design has a mass of 1.1 kg and can achieve a peak joint torque up to 108 Nm with a maximum angular velocity of 5.2 rad/s. This torque-controllable SEA was incorporated with a novel user interface capable of transferring hip joint torque during dynamic movement while maintaining high efficiency. We utilized a user state-based PID controller, which integrates the user's state such as walking speed and locomotion mode, allowing us to achieve a high fidelity closed-loop torque control during diverse walking conditions. Our study results provide meaningful contributions to the exoskeleton community in developing the next-generation wearable system for human augmentation during dynamic movements.

Acknowledgment

The authors thank Henry Luk for the initial development of the low-level controller, Alex Yu and Dawit Lee for helping out with implementing the FPGA code, and Julian Park for fabricating the exoskeleton hardware. This work was supported by the NSF NRI Award #1830215.

References

[1] Young, A. J., and Ferris, D. P., 2017. "State of the art and future directions for lower limb robotic exoskeletons". IEEE Transactions on Neural Systems and Rehabilitation Engineering, **25**(2), Feb, pp. 171–182.

[2] Sawicki, G. S., Beck, O. N., Kang, I., and Young, A. J., 2020. "The exoskeleton expansion: improving walking and running economy". Journal of NeuroEngineering and Rehabilitation, **17**(1), pp. 1–9.

[3] Kim, J., Lee, G., Heimgartner, R., Revi, D. A., Karavas, N., Nathanson, D., Galiana, I., Eckert-Erdheim, A., Murphy, P., Perry, D., et al., 2019. "Reducing the metabolic rate of walking and running with a versatile, portable exosuit". Science, **365**(6454), pp. 668–672.

[4] Zhang, J., Fiers, P., Witte, K. A., Jackson, R. W., Poggensee, K. L., Atkeson, C. G., and Collins, S. H., 2017. "Human-in-the-loop optimization of exoskeleton assistance during walking". Science, **356**(6344), pp. 1280–1284.

[5] Fontana, M., Vertechy, R., Marcheschi, S., Salsedo, F., and Bergamasco, M., 2014. "The body extender: A full-body exoskeleton for the transport and handling of heavy loads". IEEE Robotics & Automation Magazine, **21**(4), pp. 34–44.

[6] Yu, H., Choi, I. S., Han, K.-L., Choi, J. Y., Chung, G., and Suh, J., 2018. "Development of a upper-limb exoskeleton robot for refractory construction". Control Engineering Practice, **72**, pp. 104–113.

[7] Seo, K., Lee, J., Lee, Y., Ha, T., and Shim, Y., 2016. "Fully autonomous hip exoskeleton saves metabolic cost of walking". In 2016 IEEE International Conference on Robotics and Automation (ICRA), IEEE, pp. 4628–4635.

[8] Lee, D., Mclain, B. J., Kang, I., and Young, A., 2021. "Biomechanical comparison of assistance strategies using a bilateral robotic knee exoskeleton". IEEE Transactions on Biomedical Engineering.

[9] Jang, J., Kim, K., Lee, J., Lim, B., and Shim, Y., 2016. "Assistance strategy for stair ascent with a robotic hip exoskeleton". In 2016 IEEE/RSJ International Conference on Intelligent Robots and Systems (IROS), IEEE, pp. 5658–5663.

[10] Awad, L. N., Bae, J., O'donnell, K., De Rossi, S. M., Hendron, K., Sloot, L. H., Kudzia, P., Allen, S., Holt, K. G., Ellis, T. D., et al., 2017. "A soft robotic exosuit improves walking in patients after stroke". Science translational medicine, **9**(400).

[11] Quintero, H. A., Farris, R. J., and Goldfarb, M., 2012. "A method for the autonomous control of lower limb

exoskeletons for persons with paraplegia". Journal of medical devices, **6**(4).

[12] Bae, J., Siviy, C., Rouleau, M., Menard, N., O'Donnell, K., Geliana, I., Athanassiu, M., Ryan, D., Bibeau, C., Sloot, L., et al., 2018. "A lightweight and efficient portable soft exosuit for paretic ankle assistance in walking after stroke". In 2018 IEEE International Conference on Robotics and Automation (ICRA), IEEE, pp. 2820–2827.

[13] Heo, U., Kim, S. J., and Kim, J., 2020. "Backdrivable and fully-portable pneumatic back support exoskeleton for lifting assistance". IEEE Robotics and Automation Letters, **5**(2), pp. 2047–2053.

[14] Zoss, A. B., Kazerooni, H., and Chu, A., 2006. "Biomechanical design of the berkeley lower extremity exoskeleton (bleex)". IEEE/ASME Transactions on mechatronics, **11**(2), pp. 128–138.

[15] Browning, R. C., Modica, J. R., Kram, R., and Goswami, A., 2007. "The effects of adding mass to the legs on the energetics and biomechanics of walking". Medicine & Science in Sports & Exercise, **39**(3), pp. 515–525.

[16] Pratt, G. A., and Williamson, M. M., 1995. "Series elastic actuators". In Proceedings 1995 IEEE/RSJ International Conference on Intelligent Robots and Systems. Human Robot Interaction and Cooperative Robots, Vol. 1, IEEE, pp. 399–406.

[17] Pratt, J., Krupp, B., and Morse, C., 2002. "Series elastic actuators for high fidelity force control". Industrial Robot: An International Journal.

[18] Kong, K., Bae, J., and Tomizuka, M., 2009. "Control of rotary series elastic actuator for ideal force-mode actuation in human–robot interaction applications". IEEE/ASME transactions on mechatronics, **14**(1), pp. 105–118.

[19] Kong, K., Bae, J., and Tomizuka, M., 2011. "A compact rotary series elastic actuator for human assistive systems". IEEE/ASME transactions on mechatronics, **17**(2), pp. 288–297.

[20] Giovacchini, F., Vannetti, F., Fantozzi, M., Cempini, M., Cortese, M., Parri, A., Yan, T., Lefeber, D., and Vitiello, N., 2015. "A light-weight active orthosis for hip movement assistance". Robotics and Autonomous Systems, **73**, pp. 123–134.

[21] Veneman, J. F., Ekkelenkamp, R., Kruidhof, R., van der Helm, F. C., and van der Kooij, H., 2006. "A series elastic-and bowden-cable-based actuation system for use as torque actuator in exoskeleton-type robots". The international journal of robotics research, **25**(3), pp. 261–281.

[22] Kim, S., and Bae, J., 2017. "Force-mode control of rotary series elastic actuators in a lower extremity exoskeleton using model-inverse time delay control". IEEE/ASME Transactions on Mechatronics, **22**(3), pp. 1392–1400.

[23] Shepherd, M. K., and Rouse, E. J., 2017. "Design and validation of a torque-controllable knee exoskeleton for sit-to-stand assistance". IEEE/ASME Transactions on Mechatronics, **22**(4), pp. 1695–1704.

[24] Yandell, M. B., Quinlivan, B. T., Popov, D., Walsh, C., and Zelik, K. E., 2017. "Physical interface dynamics alter how robotic exosuits augment human movement: implications for optimizing wearable assistive devices". Journal of neuroengineering and rehabilitation, **14**(1), pp. 1–11.

[25] Yandell, M. B., Ziemnicki, D. M., McDonald, K. A., and Zelik, K. E., 2020. "Characterizing the comfort limits of forces applied to the shoulders, thigh and shank to inform exosuit design". Plos one, **15**(2), p. e0228536.

[26] Lee, S. E., Kilpatrick, C., Kang, I., Hsu, H., Childers, W. L., and Young, A., 2020. "Investigating the impact of the user interface for a powered hip orthosis on metabolic cost and user comfort: a preliminary study". JPO: Journal of Prosthetics and Orthotics.

[27] Yan, T., Cempini, M., Oddo, C. M., and Vitiello, N., 2015. "Review of assistive strategies in powered lower-limb orthoses and exoskeletons". Robotics and Autonomous Systems, **64**, pp. 120–136.

[28] Zhang, J., Cheah, C. C., and Collins, S. H., 2017. "Torque control in legged locomotion". In Bioinspired Legged Locomotion. Elsevier, pp. 347–400.

[29] Bovi, G., Rabuffetti, M., Mazzoleni, P., and Ferrarin, M., 2011. "A multiple-task gait analysis approach: kinematic, kinetic and emg reference data for healthy young and adult subjects". Gait & posture, **33**(1), pp. 6–13.

[30] Winter, D. A., 1984. "Kinematic and kinetic patterns in human gait: variability and compensating effects". Human movement science, **3**(1-2), pp. 51–76.

[31] Camargo, J., Ramanathan, A., Flanagan, W., and Young, A., 2021. "A comprehensive, open-source dataset of lower limb biomechanics in multiple conditions of stairs, ramps, and level-ground ambulation and transitions". Journal of Biomechanics, p. 110320.

[32] Fryar, C. D., Carroll, M. D., Gu, Q., Afful, J., and Ogden, C. L., 2021. "Anthropometric reference data for children and adults: United states, 2015-2018".

[33] Irmscher, C., Woschke, E., May, E., and Daniel, C., 2018. "Design, optimisation and testing of a compact, inexpensive elastic element for series elastic actuators". Medical engineering & physics, **52**, pp. 84–89.

[34] Paine, N., Mehling, J. S., Holley, J., Radford, N. A., Johnson, G., Fok, C.-L., and Sentis, L., 2015. "Actuator control for the nasa-jsc valkyrie humanoid robot: A decoupled dynamics approach for torque control of series elastic robots". Journal of field robotics, **32**(3), pp. 378–396.

[35] Zhang, T., Tran, M., and Huang, H., 2018. "Design and experimental verification of hip exoskeleton with balance capacities for walking assistance". IEEE/ASME Transactions On Mechatronics, **23**(1), pp. 274–285.

[36] Kang, I., Kunapuli, P., Hsu, H., and Young, A. J., 2019. "Electromyography (emg) signal contributions in speed and slope estimation using robotic exoskeletons". In 2019 IEEE 16th International Conference on Rehabili-

tation Robotics (ICORR), IEEE, pp. 548–553.

[37] Kang, I., Hsu, H., and Young, A., 2019. "The effect of hip assistance levels on human energetic cost using robotic hip exoskeletons". IEEE Robotics and Automation Letters, **4**(2), pp. 430–437.

[38] Kang, I., Molinaro, D. D., Duggal, S., Chen, Y., Kunapuli, P., and Young, A. J., 2021. "Real-time gait phase estimation for robotic hip exoskeleton control during multimodal locomotion". IEEE Robotics and Automation Letters, **6**(2), pp. 3491–3497.

[39] Lee, J., Seo, K., Lim, B., Jang, J., Kim, K., and Choi, H., 2017. "Effects of assistance timing on metabolic cost, assistance power, and gait parameters for a hip-type exoskeleton". In 2017 International Conference on Rehabilitation Robotics (ICORR), IEEE, pp. 498–504.

[40] Ding, Y., Panizzolo, F. A., Siviy, C., Malcolm, P., Galiana, I., Holt, K. G., and Walsh, C. J., 2016. "Effect of timing of hip extension assistance during loaded walking with a soft exosuit". Journal of neuroengineering and rehabilitation, **13**(1), p. 87.

[41] Lim, B., Lee, J., Jang, J., Kim, K., Park, Y. J., Seo, K., and Shim, Y., 2019. "Delayed output feedback control for gait assistance with a robotic hip exoskeleton". IEEE Transactions on Robotics.

[42] Tanaka, N., Matsushita, S., Sonoda, Y., Maruta, Y., Fujitaka, Y., Sato, M., Simomori, M., Onaka, R., Harada, K., Hirata, T., et al., 2019. "Effect of stride management assist gait training for poststroke hemiplegia: a single center, open-label, randomized controlled trial". Journal of Stroke and Cerebrovascular Diseases, **28**(2), pp. 477–486.

Supplemental Document

Simulation of the Series Elastic Actuator Operating Voltage

One of the key actuator design criteria when developing an exoskeleton is the optimization of the operating voltage. Conventionally, this operating voltage does not vary as the output shaft is often locked (minimal change in the velocity) during torque control. Conversely, in exoskeleton applications during locomotion, the actuator rotor is constantly back-driven by the user. This phenomenon leads to an unwanted back EMF voltage around the motor armature causing voltage fluctuations in the motor driver. To ensure a safe operation of our exoskeleton, we simulated our SEA voltage response during different walking conditions. The governing equation that dictates the motor voltage is

$$V_m = \frac{\tau_m}{k_t} R_m + k_e \omega_m \tag{1}$$

where V_m is the motor voltage, τ_m is the motor torque, k_t is the motor torque constant, R_m is the motor winding resistance, k_e is the motor voltage constant, and ω_m is the joint angular velocity.

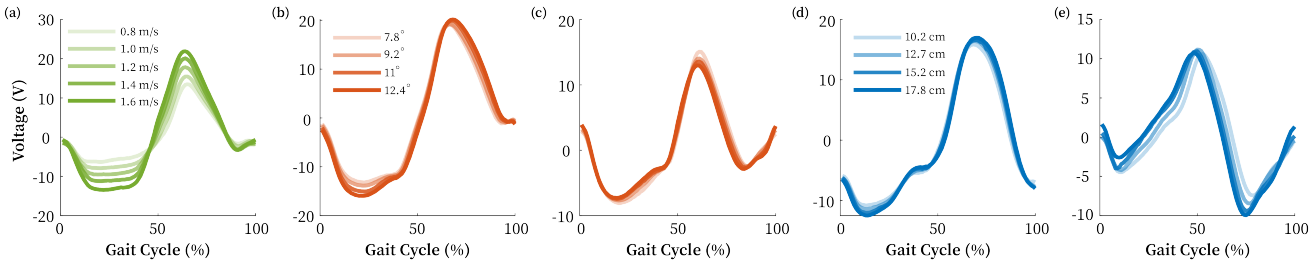

Supp. Fig. 1. Simulation of the series elastic actuator operating voltage across different walking conditions. (A) Level-Ground, (B) Ramp Ascent, (C) Ramp Descent, (D) Stair Ascent, and (E) Stair Descent.

Along with this equation, we utilized human gait biomechanics data (biological joint moment and joint angular velocity) to calculate the actuator voltage across different walking speeds (0.8 m/s $\sim$ 1.6 m/s) and ambulation modes (LG, RA, RD, SA, and SD) (Supp. Fig. 1). For ramps and stairs, we included terrain contexts that followed the Americans with Disabilities Act Accessibility Standards for building construction (ramp, 7.8° $\sim$ 12.4° and stair, 10.2 cm $\sim$ 17.8 cm). Using the SEA gear ratio, we calculated the required τ_m and ω_m and other variables (k_t, R_m, and k_e) were obtained from the manufacturer's datasheet. We assumed that the exoskeleton user had a body mass (90 kg) of an average male in the United States and the assistance level was set to 100% of the user's biological hip joint moment. Our Simulation results indicated that our SEA does not exceed our operating voltage (24 V) across all walking conditions.